Utrecht University

TU Delft

UTRECHT UNIVERSITY

MSc CLIMATE PHYSICS

DELFT UNIVERSITY OF TECHNOLOGY

MSc HYDRAULIC ENGINEERING

A new convective model of the Weddell Polynya

Author:

D.B. Boot

6077366

Supervisors:

Prof. Dr. Ir. H.A. Dijkstra (UU)

R.M. van Westen, MSc (UU)

Dr. C.A. Katsman (DUT)

June, 2019

Abstract

The Weddell Polynya, a large hole in the Antarctic sea ice, reappeared in 2017. The polynya forms due to deep convection, which is caused by static instability of the water column. Observations and model studies show periodic heat accumulation in the subsurface layer prior to a polynya. This heat accumulation could be caused by internal ocean dynamics: the Southern Ocean Mode. Periodic subsurface heat and salt accumulation could be the major driver in causing periodic deep convection, which is in contrast with earlier studies. These studies focus on surface processes, and see the polynya as an irregular event. In this study a simple convective model is used to look into this contrast. Model simulations excluding and including periodic subsurface heat and salt fluxes have been performed. Multiple polynya events were only simulated in the model set up including subsurface fluxes. The dominant frequency for polynya events in these simulations equals the frequency of the subsurface heat and salt accumulation. This frequency is still visible in runs with white noise added to the freshwater flux, showing the importance and dominance of the subsurface forcing. In combination with earlier studies, this study suggests that periodic subsurface processes are most dominant and govern the initial formation and periodicity of the Weddell Polynya.

1 Introduction

The Weddell Polynya (WP), a large hole in the sea ice surrounding Antarctica, reappeared in 2017. During austral winter the WP forms approximately 800km offshore and is, unlike coastal polynyas, completely enclosed by sea ice. Polynyas typically form in the Maud Rise region around 65°S and 0°E (Fig. 1) (Martinson et al., 1981). The first polynyas were observed in the 1970s with newly available satellite images (Carsey, 1980). In 1974, 1975, and 1976 polynyas were present during the entire winter with an areal extent of approximately 2.5×10^5 km^2 (Gordon, Viscbeck and Comiso, 2007). In 2017 the WP reappeared with an approximate area of 0.5×10^5 km^2 (Cheon and Gordon, 2019). Observations also suggest a short-lived polynya in 1994 (Holland, 2001).

After the first observed polynya events in the 1970s several studies have looked into the processes leading to the formation of the WP. To melt ice with an area as large as the WP a large amount of heat is necessary. Martinson et al. (1981) used a simple 1D vertical convective model to show that deep convection is the only process that is able to supply this amount of heat. They conclude that deep convection is caused by brine rejection and that the period of deep convection is irregular. They also state that the preconditioning of the ocean in this region is an important factor. However, the processes governing the preconditioning of the ocean remain less clear, and suggestions for other processes, such as atmospheric processes, causing the deep convection have been made. Parkinson (1983) showed that polynya formation is dependent on the wind field, and not only caused by oceanographic processes. With a constant ocean heat flux, she showed

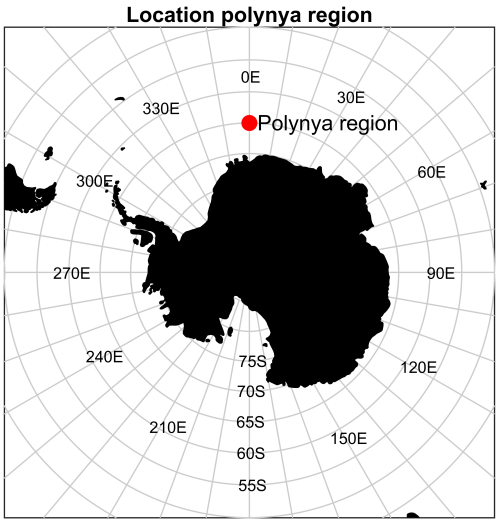

Fig. 1: Location of the polynya region (65°S. 0°E).

that a polynya can form in the middle of a cyclonic wind field. This is the effect of a divergent stress in the ice caused by the wind field. In Francis et al. (2019) it is suggested that the origin of the 2017 event is purely dynamical instead of thermodynamical. During austral winter in 2017 there were unusual frequent and intense cyclones present above the polynya region. In Gordon et al. (2007) it is suggested that a persisting negative Southern Annular Mode (SAM) leads to drier than usual conditions in the Southern Ocean. This results in a saltier than usual top layer, and a weaker than usual stratification. The reduced stratification preconditions the ocean, and in combination with a La Niña event (increased sea ice formation, and thus increased brine rejection) deep convection could be induced. Cheon and Gordon (2019) used the SAM to explain the difference in size between the 1970s polynya and the 2017 event. Besides atmospheric processes, dynamical processes have also been mentioned. Holland (2001) used a coupled sea-ice general circulation model with an idealised seamount to show the effect of eddy shedding at the flanks of Maud Rise on the sea ice. The flow impinging on Maud Rise gains cyclonic vorticity at the northeastern flank due to vortex stretching. This results in a divergent stress on the sea ice, which opens the ice pack. In this opening atmospheric, thermodynamical feedbacks cool the surface layer, making it denser, with could result in deep convection. Another topographically induced effect is Taylor cap dynamics. A Taylor cap is a dome of water above a seamount with almost no interactions with its surroundings. It weakens the stratification above the seamount (Alverson and Owens, 1996; Kurtakoti et al., 2018), making it more vulnerable for static instability. Through these dynamical effects, Maud Rise also influences the sea ice. This effect is visible in observations of a halo of low ice concentrations over the flanks of Maud Rise (Lindsay et al., 2004). The atmospheric and dynamicals processes all have an impact on polynyas. What they have in common, is that they mostly focus on surface processes. Furthermore, these processes do not show a dominant period for the WP.

Improved climate models also give us the opportunity to study deep convection and WP events in the Southern Ocean. Several studies have been performed using different climate models. These studies showed a multidecadal to a multicentennial periodicity for the WP (Martin, Park and Latif, 2013; Zanowski, Hallberg and Sarmiento, 2015; Latif, Martin, Reintges and Park, 2017; Weijer et al., 2017). One of the models, the Kiel Climate Model (KCM), shows a build up of heat in the subsurface layer. This build up of heat is essential for polynya formation. Through buoyancy gain of the subsurface layer, deep convection is induced, which results in polynya formation (Martin et al., 2013; Latif et al., 2017; Reintges et al., 2017). Stratification is shown to be important in the model studies of Latif et al. (2017) and Reintges et al. (2017). They state that in the KCM a stronger stratification results in a longer periodicity, because more buoyancy gain is necessary to overcome the

more stable stratification. In addition, Weijer et al. (2017) showed the importance of the resolution of the climate model. In their high resolution run (0.1°) polynyas were observed, whereas in the low resolution run (1°) no polynyas were simulated. This is confirmed by Dufour et al. (2017) using the GFDL CM2-O model with a nominal ocean grid spacing of 0.25 $^\circ$ and 0.1°. In their study they show deep convection is not sufficient to create polynyas. It is important that the subsurface heat reservoir can supply enough heat to melt all of the sea ice. Therefore it is important that the stratification is strong enough to allow for the build up of heat. Resolution of the models, in both the horizontal grid and the bathymetry, is an important factor, because the ability of a model to represent restratifying, mesoscale eddies, determines in part the strength of the stratification. The restratifying effect of the mesoscale eddies results in more heat build up in the subsurface layer. Therefore higher resolution models allow for more heat accumulation which is shown to be important for polynya formation. These higher resolution models also approach the observed periodicity of the WP (20 or 40, if not counting the 1994 event, years) best. These studies show the importance of subsurface processes for the Weddell Polynya, and moreover, they also show a dominant periodicity.

From these model studies two conclusions can be drawn: both resolution and heat accumulation are important factors for representing polynyas. A model study of van Westen and Dijkstra (2019) suggested a process for this heat accumulation: they relate the accumulation of heat to the Southern Ocean Mode (SOM), a multidecadal mode of intrinsic variability of sea surface temperature in the Southern Ocean caused by eddy-mean flow interactions (Jüling et al., 2018). The SOM was identified by Le Bars, Viebahn and Dijkstra (2016) in an eddying version of the Parallel Ocean Program (POP). In Le Bars et al. (2016) and in a Community Earth System Model (CESM) simulation of van Westen and Dijkstra (2017) the SOM was identified with a 40 year period. In an extended run of van Westen and Dijkstra (2017), further adjustment of the model resulted in a period of 25 years (van Westen and Dijkstra, 2019). This approaches the observed periodicity of the WP of 20 years. In this simulation, a correlation was found between the SOM and the presence of the WP. They suggested that heat content anomalies propagate from the SOM region (50°S - 35°S, 50°W - 0°W) via the Antarctic Circumpolar Current (ACC) to 30°E where they enter the Weddell Gyre as Warm Deep Water (WDW). The anomalies propagate towards the polynya area near Maud Rise where they can induce deep convection. The lag between a positive SOM phase and a polynya event is of the same order as the time necessary to propagate from the SOM region to the polynya region with the ambient current (10 years). van Westen and Dijkstra (2019) suggested that the WP is part of this intrinsic variability of the climate system and that the deep convection related to the WP is mainly caused by

subsurface heat transport.

Even though many studies investigated the origin of the WP, there is no consensus on the importance of the different processes as well as the periodicity of the WP. Several studies have focused on surface processes without a clear dominant periodicity (e.g. Martinson et al., 1981; Holland, 2001; Gordon et al., 2007), while studies with (high resolution) climate models show the importance of subsurface processes with a dominant multidecadal frequency. Though all processes can be important for the size, location and duration of the WP, it is not clear what the most dominant process for the initial formation, and the periodicity of the WP is. In an earlier study of Martinson et al. (1981) the WP was marked as an irregular occurring event caused by brine rejection in a preconditioned ocean. The high resolution CESM simulation of van Westen and Dijkstra (2019) shows a periodic return of the WP due to periodic heat accumulation in the subsurface layer. The contrast between the simple model of Martinson et al. (1981) and the high resolution simulation of van Westen and Dijkstra (2019) is a reason to revisit the original model of Martinson et al. (1981) and to use this model to look into two issues: what is the importance of surface forcing relative to subsurface forcing, and what governs the periodicity of the WP? To look into these issues, first an attempt is made to reproduce the results of Martinson et al. (1981). This model was used to investigate the 1970s polynya. We will test whether multiple events (e.g. the 1970s and 2017 event) can be explained using this model. Secondly, the original model is extended with a dynamical subsurface layer instead of a constant subsurface layer, since observations (Fahrbach et al., 2011), and several climate models (Martin et al., 2013; Latif et al., 2017; Reintges et al., 2017; Kurtakoti et al., 2018; van Westen and Dijkstra, 2019) show an accumulation of heat (and salt) prior to a WP event. Heat and salt fluxes are used to force the subsurface layer. This extended version of the Martinson model is described in Section 2. The results are discussed in Section 3, and in Section 4 a summary and discussion of the results is given.

2 Model

The model used in this study is an extended version of the model used in Martinson et al. (1981). The model is extended with an active subsurface layer, and horizontal advective fluxes in both the surface and the subsurface layer. First the model is described, after which the experimental set up and parameter values are discussed.

2.1 Model description

The used model is a simple one-dimensional, vertical model with two layers of constant depth and uniform temperature, salinity and density.The model simulates the development of temperature (T), salinity (S), and sea ice thickness (δ) under surface and subsurface forcing. The model has four different regimes, which are differentiated on ice cover (ice free versus ice covered) and static stability (stable, two layered versus unstable, mixed). There are the ice free regimes 1 and 2, and the ice covered regimes 3 and 4. Regimes 2 and 4 are stable ($\rho_1 < \rho_2$), and regimes 1 and 3 are mixed with one uniform layer over the entire depth (Fig. 2).

The model transits through these four regimes. The different regime transitions are displayed with arrows in Fig. 2. There are four different regime transitions: (1) from ice covered regimes to ice free regimes due to complete melt of the sea ice ($\delta = 0$) (regime 4 to 2 and regime 3 to 1); (2) from ice free regimes to ice covered regimes, because the surface layer reaches freezing temperature and sea ice starts to form ($T_1 = T_f$) (regime 2 to 4, and regime 1 to 3); (3) from stable, two layered regimes to unstable, mixed regimes, because the density of the surface layer is equal to or larger than the density of the subsurface layer ($\rho_1 \geq \rho_2$) (regime 2 to 1, and regime 4 to 3); (4) from unstable, mixed regimes to stable, two layered regimes, because of stabilisation of the water column due to a decreasing density of the mixed layer ($-\alpha\frac{dT}{dt} + \beta\frac{dS}{dt} < 0$) (regime 1 to 2, and regime 3 to 4).

The model is forced at the surface by a freshwater flux ($F = (P - E) \times 35$ g/kg), and a monthly varying heat flux (Q_{ia} for ice covered regimes and Q_{oa} for open ocean regimes). Both the surface and subsurface layer are subject to a horizontal advective heat and salt flux (F_{T1} and F_{S1} for the surface layer, and F_{T2} and F_{S2} for the subsurface layer) which depend on a background value (T_{b1} and S_{b1} for the surface layer, and T_{b2} and S_{b2} for the subsurface layer) and a relaxation timescale (τ).

Between the two layers, heat and salt transfer is modelled using exchange coefficients (K_T and K_S) which account for upwelling, turbulent exchange and diffusion. In ice covered regimes there is a heat flux present between the sea ice and the underlying layer. This flux is modelled using a turbulent exchange coefficient (K). During ice growth, brine is rejected, and during ice melt, fresh water is added to the surface layer. Brine rejection and melt is modelled using a constant representing the salinity difference between sea ice and seawater (σ), and the rate of ice growth ($\frac{d\delta}{dt}$).

For each regime there is a set of equations determining the temperature and salinity per layer, and the sea ice thickness which represent these processes (Equations 1 to 4). The density per layer is determined with a simple linear equation of state (Equation 5). This equation neglects nonlinear and pressure dependent terms. The differences between

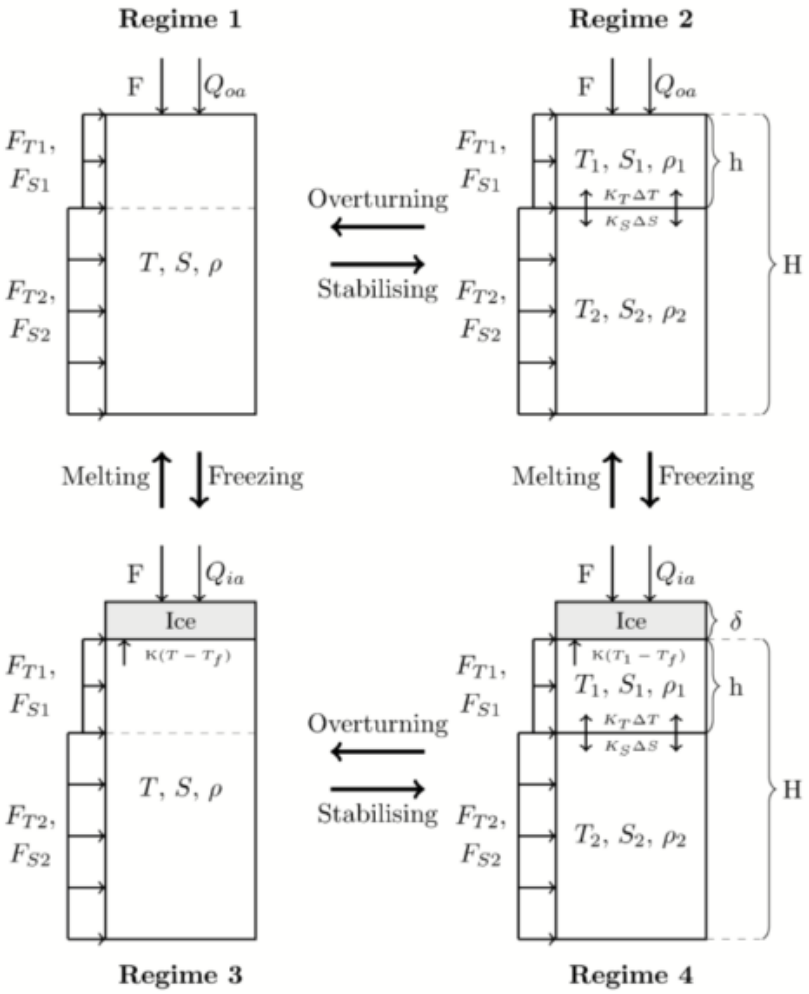

Fig. 2: A schematic representation of the different regimes of the model. This model is an extension of the model used in Martinson et al. (1981). The different parameters are mentioned and explained in the text. The directions and size of the arrows are not a representation of the actual direction and magnitude of the fluxes. Positive fluxes represent fluxes entering the system. Regime transitions are shown by bold arrows.

the linear equation and more complicated versions are irrelevant for this study, because the density difference is only determined at the interface between the layers (Martinson et al., 1981).

Regime 1:

$$H\frac{dT}{dt} = \frac{Q_{oa}}{\rho_0 C_p} + \tau(T_{b1} - T)h + \tau(T_{b2} - T)(H - h) \tag{1a}$$

$$H\frac{dS}{dt} = -F + \tau(S_{b1} - S)h + \tau(S_{b2} - S)(H - h) \tag{1b}$$

$$\delta = 0 \tag{1c}$$

Regime 2:

$$h\frac{dT_1}{dt} = \frac{Q_{oa}}{\rho_0 C_p} + K_T(T_2 - T_1) + \tau(T_{b1} - T_1)h \tag{2a}$$

$$h\frac{dS_1}{dt} = K_S(S_2 - S_1) - F + \tau(S_{b1} - S_1)h \tag{2b}$$

$$\delta = 0 \tag{2c}$$

$$\frac{dT_2}{dt} = \tau(T_{b2} - T_2) + \frac{K_T(T_1 - T_2)}{H - h} \tag{2d}$$

$$\frac{dS_2}{dt} = \tau(S_{b2} - S_2) + \frac{K_S(S_1 - S_2)}{H - h} \tag{2e}$$

Regime 3:

$$H\frac{dT}{dt} = K(T - T_f) + \tau(T_{b1} - T)h + \tau(T_{b2} - T)(H - h) \tag{3a}$$

$$H\frac{dS}{dt} = \sigma\frac{d\delta}{dt} - F + \tau(S_{b1} - S)h + \tau(S_{b2} - S)(H - h) \tag{3b}$$

$$\frac{d\delta}{dt} = \frac{1}{\rho_i L}(-Q_{ia} - \rho_0 C_p K(T - T_f)) + \frac{F}{\sigma} \tag{3c}$$

Regime 4:

$$h\frac{dT_1}{dt} = K_T(T_2 - T_1) - K(T_1 - T_f) + \tau(T_{b1} - T_1)h \tag{4a}$$

$$h\frac{dS_1}{dt} = \sigma\frac{d\delta}{dt} - F + \tau(S_{b1} - S_1)h \tag{4b}$$

$$\frac{d\delta}{dt} = \frac{1}{\rho_i L}(-Q_{ia} - \rho_0 C_p K(T_1 - T_f)) + \frac{F}{\sigma} \tag{4c}$$

$$\frac{dT_2}{dt} = \tau(T_{b2} - T_2) + \frac{K_T(T_1 - T_2)}{H - h} \tag{4d}$$

$$\frac{dS_2}{dt} = \tau(S_{b2} - S_2) + \frac{K_S(S_1 - S_2)}{H - h} \tag{4e}$$

Equation of state:

$$\frac{\rho - \rho_0}{\rho_0} = -\alpha T + \beta S \tag{5}$$

In these equations C_p is the specific heat of seawater with density ρ_0. Ice has a density of ρ_i and latent heat L. The depth of the entire column is H, with a smaller top layer with depth h. α and β are constants in the equation of state representing thermal and haline contraction, respectively.

In the model, a regime change can also change the initial conditions for the new regime. The new initial conditions are indicated with a prime. Horizontal bars above a variable represent averaging over the water column due to overturning: $\bar{X} = (hX_1 + (H-h)X_2)/H$,

where X is either T or S.

$$\text{regime 1} \rightarrow \text{regime 2 if } -\alpha\frac{dT}{dt} + \beta\frac{dS}{dt} < 0;$$
$$T_1' = T,\ S_1' = S,\ \delta' = 0;$$
$$\text{regime 1} \rightarrow \text{regime 3 if } T = T_f;$$
$$T' = T_f,\ S' = S,\ \delta' = 0;$$
$$\text{regime 2} \rightarrow \text{regime 1 if } \rho_1 = \rho_2;$$
$$T' = \bar{T},\ S' = \bar{S},\ \delta' = 0;$$
$$\text{regime 2} \rightarrow \text{regime 4 if } T_1 = T_f;$$
$$T_1' = T_1,\ S_1' = S_1,\ \delta' = 0;$$
$$\text{regime 3} \rightarrow \text{regime 1 if } \delta = 0;$$
$$T' = T,\ S' = S,\ \delta' = 0;$$
$$\text{regime 3} \rightarrow \text{regime 4 if } -\alpha\frac{dT}{dt} + \beta\frac{dS}{dt} < 0;$$
$$T_1' = T,\ S_1' = S,\ \delta' = \delta;$$
$$\text{regime 4} \rightarrow \text{regime 2 if } \delta = 0;$$
$$T_1' = T_1,\ S_1' = S_1,\ \delta' = 0;$$
$$\text{regime 4} \rightarrow \text{regime 3 if } \rho_1 = \rho_2;$$
$$T' = \bar{T},\ S' = \bar{S},\ \delta' = \delta;$$

It should be noted that for the model to switch between regimes 1 and 3 the entire water column should reach freezing temperature, which is physically not realistic. This condition is therefore never met.

The set of differential equations is solved using the ODE15s solver incorporated in Matlab. The ODE15s solver is a variable-step, variable-order solver based on an algorithm by Klopfenstein (1971) using numerical differentiation formulas (NDFs) orders 1 to 5. Tolerances for the absolute and relative error are used to increase the accuracy of the model. These tolerances are 10^{-10} and 10^{-8}, respectively. The absolute error tolerance measures when the solution becomes unimportant. The relative error tolerance is the size of the allowable error relative to the magnitude of the solution.

2.2 Experimental set up

The model described in section 2.1 is used using two different set ups ('Martinson' and 'Extended'). The 'Extended' set up uses all model components, while in the 'Martinson' set up several components are switched off. The differences between the two set ups, are displayed in Tab. 1. The 'Martinson' set up has two different cases (REF.1 and REF.2). The 'Subsurface' set up has three (SSB, SST, and SSS).

Tab. 1: The different model components, and values for K_T and K_S per case. A model component can either be included ('on'), or excluded ('off'). The model component 'dynamic T_2 and S_2' stands for an active subsurface layer. If this component is excluded, the set up uses a constant subsurface layer. If either F_{T2} or F_{S2} is excluded, the background value corresponding to the flux is set constant. The model components containing 'F' represent the horizontal heat (T) and salt (S) fluxes in either the surface (1), or subsurface (2) layer.

Model component	Martinson		Subsurface		
	REF.1	REF.2	SSB	SST	SSS
Dynamic T_2 and S_2	off	off	on	on	on
F_{T1}, F_{S1}	off	off	on	on	on
F_{T2}	off	off	on	on	off
F_{S2}	off	off	on	off	on
K_T [10^{-6}m s^{-1}]	5.00	5.00	2.82	2.80	2.80
K_S [10^{-6}m s^{-1}]	1.375	2.00	2.82	2.80	2.80

The 'Martinson' set up uses the original model of Martinson et al. (1981). The horizontal advective fluxes (F_{T1}, F_{S1}, F_{T2} and F_{S2}) are switched off, and the subsurface layer is set on a constant value. Two different cases (REF.1 and REF.2) are used which use a different value for K_S. A higher value of K_S results in more salt transfer from the subsurface layer to the surface layer, increasing the density of the surface layer, making it more prone to overturning. Two cases are used because of the completely different behaviour of the cases. REF.1 uses a lower K_S and REF.2 a higher K_S. This means that REF.2 is more prone to show deep convection. With this set up, an attempt is made to reproduce the original results of Martinson et al. (1981). Compared to Martinson et al. (1981) longer runs are used to investigate the long term behaviour of the model.

The 'Extended' set up uses a dynamic subsurface layer and horizontal advective fluxes as described in section 2.1. The three cases are differentiated on the inclusion of the different components of the subsurface forcing. Case SSB (subsurface both) uses both a subsurface heat and salt flux. Case SST (subsurface temperature) uses only a subsurface heat flux. The subsurface salt flux is set constant. Case SSS (subsurface salinity) uses only a salt flux, and the heat flux is set constant. The aim of this set up is to reproduce the general features of the CESM simulation of van Westen and Dijkstra (2019), where the observed periodicity of the WP events is one of the key features. The different cases are used to assess the importance of the different components of the subsurface forcing.

Cases REF.1 and SSB have also been tested with white noise added to the freshwater flux (F). The aim of these tests is to investigate the influence of noise on the regularity of polynya events. For case SSB the main question is whether the same dominant frequency is still visible. For REF.1 the effect of noise on inducing deep convection is assessed.

Parameter values per case are displayed in Tab. 2. The parameter values are either

taken from Martinson et al. (1981), or based on the CESM simulation of van Westen and Dijkstra (2019), or they are determined through tuning of the model. The aim of the model is to look into multiple polynya events, therefore it is necessary to tune the model into simulating multiple events. The forcing of the model (the horizontal fluxes, surface heat fluxes, and freshwater flux), is displayed in Section 3.

The typical depth of the layers have been determined from the CESM simulation of van Westen and Dijkstra (2019). The depth of the surface layer (h) is set to 160m, because in CESM potential density data shows a clear homogeneous layer below 160m (not shown). This compares well to the value used in Kurtakoti et al. (2018) (150m), but is smaller than the value used in Martinson et al. (1981) (200m). The depth of the entire layer (H) is set on 2000m. This is the approximate mixed layer depth during convective events in the CESM simulation. This magnitude corresponds well to values presented in Fahrbach et al. (2011) for the depth of WDW, and in Dufour et al. (2017). It is however half the size of the value used in Martinson et al. (1981) (4000m).

The turbulent exchange coefficient K, and the exchange coefficients K_T and K_S have been used as tuning parameters for the different cases. K was set to 1×10^{-4} ms^{-1} for all cases (in Martinson et al. (1981) this value was 3×10^{-4} ms^{-1}). For the Martinson set up, double diffusive processes are important, since K_T and K_S have different values. For the subsurface set up double diffusion is not taken into account. The values per case are shown in Tab. 1. To compare the magnitude of these parameters with values used in literature the values need to be converted from ms^{-1} to m^{2}s^{-1}, which is the usual unit for vertical diffusivity parameters. This is done by multiplying these values with the depth of the surface layer (i.e. 160m). This results in values between 2.2×10^{-4} m^{2}s^{-1} and 8×10^{-4} m^{2}s^{-1}. Comparable values are found in a model study of Dufour et al. (2017) for this same location and in observations from Shaw and Stanton (2014). These values are larger than the values used in Martinson et al. (1981) ($K_T = 7 \times 10^{-7}$ ms^{-1} and $K_S = 10^{-7}$ ms^{-1}).

The adjustment time of the model to the initial conditions is a few years. Therefore the long term behaviour of the model is not sensitive to the exact initial conditions. There are two constraints on the initial conditions. Firstly, the starting regime of the model should be taken into account. If the model starts in stable regimes 2 and 4, the density of the surface layer should be lower than that of the subsurface layer. Also the ice cover should be taken into account. Ice free regimes 1 and 2 should be initiated without sea ice ($\delta = 0$), and ice covered regimes 3 and 4 should be initiated with sea ice ($\delta > 0$). And secondly, during the first years, the model is still adjusting. This adjustment time is approximately 2 years for T_1 and δ. During this period no overturning should occur due to the initial conditions. All

Tab. 2: Parameter values for constants. Superscripts show whether the parameter value is determined from the CESM simulation of van Westen and Dijkstra (2019) (C), determined through tuning (T), or taken from Martinson et al. (1981) (M). The initial conditions are chosen based on the requirements explained in the text.

Parameter	Value	Parameter	Value	Parameter	Value
h^C [m]	160	$\delta(0)$ [m]	1	C_P^M [J kg^{-1} °C^{-1}]	4.18×10^3
H^C [m]	200	α^M [°C^{-1}]	5.82×10^{-5}	L^M [J kg^{-1}]	2.5×10^5
K^T [m s^{-1}]	10^{-4}	β^M [(g/kg)$^{-1}$]	8×10^{-4}	σ^M [g/kg]	30
$T_1(0)$ [°C]	0.1	ρ_0^M [kg m^{-3}]	1000	T_f^M [°C]	-1.86
$S_1(0)$ [g/kg]	34.2	ρ_i^M [kg m^{-3}]	900		

runs are started on the 1st of January in stable regime 4.

3 Results

In this section the results are displayed. Firstly, the used forcing, determined from the CESM simulation used in van Westen and Dijkstra (2019) is discussed. Secondly, an analysis of the model behaviour is given after which the 'Martinson' set up (cases REF.1 and REF.2) is discussed. The results of the 'Extended' set up (cases SSB, SST, and SSS) are shown. And lastly, noise is added to the freshwater flux for cases REF.1 and SSB.

3.1 Forcing

All cases are forced by the same monthly varying heat flux (Q_{oa} or Q_{ia}) and freshwater flux (F) at the surface. The subsurface cases are also forced by horizontal heat and salt fluxes in both layers (FT_1, FS_1, FT_2 and FS_2). The forcing is determined from the CESM simulation used in van Westen and Dijkstra (2019). They determined a region with a probability density function where polynyas were most likely to form in there simulation (2°E - 11°E $\times$ 63.5° - 66.5°). The CESM output used for this analysis represents this region and consists of monthly values.

For the ice free regimes (1 and 2) the model is forced by an ocean-atmosphere heat flux (Q_{oa}). In the ice covered regimes (3 and 4), the ice-atmosphere heat flux (Q_{ia}) is used. The distinction between ice covered regimes and ice free regimes in the CESM simulation is based on the ice fraction. When the ice fraction in the polynya region drops below 0.5, a large increase in heat flux is observed. Therefore, if the ice fraction in this area is larger than 0.5, the regime is considered to be ice covered. When the ice fraction is smaller, the heat flux is considered to be between the ocean and the atmosphere. In months without sea ice, the ice-atmosphere flux is set equal to the ocean-atmosphere heat flux. This results

Tab. 3: Ocean-atmosphere heat flux (Q_{oa} in Wm^{-2}), ice-atmosphere heat flux (Q_{ia} in Wm^{-2}), and the freshwater input (f=P-E) in mm/day for polynya (P) and non-polynya (NP) regimes per month determined from the CESM simulation of van Westen and Dijkstra (2019). Positive values represent fluxes going into the ocean or the sea ice (warming and net precipitation). Negative values represent fluxes going to the atmosphere (cooling and net evaporation).

Month	Q_{oa}[Wm^{-2}]	Q_{ia}[Wm^{-2}]	f_P[mm/day]	f_{NP}[mm/day]
1	61.4	61.4	0.91	0.87
2	-23.6	-23.6	1.17	1.06
3	-90.8	-90.8	0.96	1.04
4	-144.1	-86.1	0.62	0.86
5	-161.3	-90.3	0.96	0.93
6	-202.3	-79.3	0.47	1.17
7	-246.9	-72.5	0.22	1.09
8	-205.6	-65.2	0.13	1.07
9	-76.9	-40.3	0.62	1.27
10	-43.0	-1.2	0.69	1.32
11	107.4	44.1	0.78	1.11
12	128.2	128.2	0.44	0.79

in the monthly heat fluxes displayed in Tab. 3. These fluxes are interpolated linearly in the model.

The presence of a polynya changes the magnitude of the freshwater flux (F) due to more evaporation. Therefore the model uses different forcing during a polynya period relative to a non-polynya period. The values for the non-polynya regime freshwater input (f_{NP}), and the polynya regime freshwater input (f_P) are presented in Tab. 3. These monthly values are interpolated linearly in the model. The total freshwater input (f) is 0.38 m $year^{-1}$ for non-polynya years, and 0.24 m $year^{-1}$ for polynya years. The first value is within the range presented in Martinson et al. (1981) (0.38-1.73 m $year^{-1}$). The value for polynya years is out of this range. However, this range is based on observations, and in 1981 no observations were available for the freshwater input during a polynya event.

For the four horizontal advective fluxes (FT_1, FS_1, FT_2 and FS_2) a background temperature (T_{b1} and T_{b2}) and salinity (S_{b1} and S_{b2}) were used. All four values were determined from the CESM simulation. For the first layer the background temperature (T_{b1}) is set on a constant $-0.33°$C. The background salinity (S_{b1}) was slightly altered to tune the model. The determined value of 34.5 g/kg was changed to 34.4814 g/kg. The background temperature and salinity of the subsurface layer (T_{b2} and S_{b2}) are periodic in nature and are shown in Fig. 3. CESM model years 210-235 were used, and the temperature and salinity are averaged over the layer between 200m and 1000m. In this layer most of the heat and salt accumulation is seen in van Westen and Dijkstra (2019).

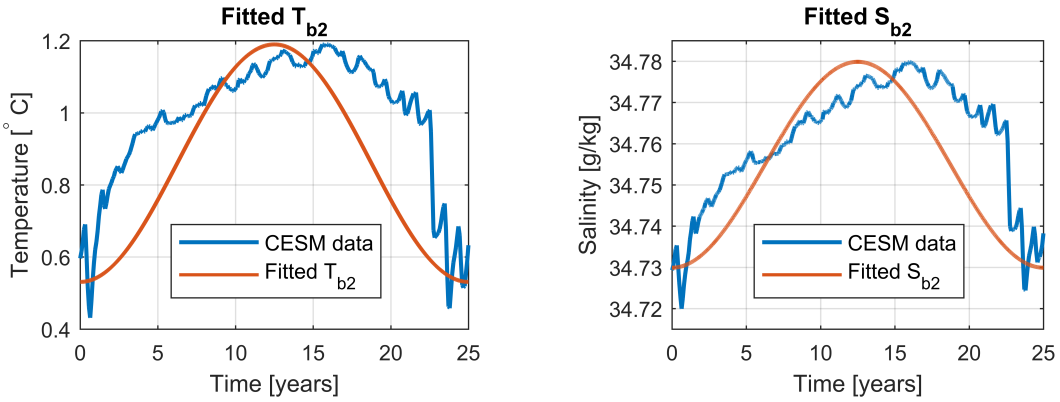

(a) T_{b2} fitted to CESM data. *(b) T_{s2} fitted to CESM data.*

Fig. 3: (a) Subsurface background temperature (T_{b2}) (red line) used in the extended model set up fitted to the CESM simulation of van Westen and Dijkstra (2019) (blue line). A sinusoidal function is fitted to CESM model years 210-235. The CESM simulation data (blue line) is averaged over depth (200-1000m). (b) Same as (a) but now for the subsurface background salinity (S_{b2}).

For all horizontal fluxes a relaxation timescale (τ) was used. This parameter was used as a tuning parameter. Eventually the value used for this time scale was $\frac{1}{200\ \text{days}}$, which is of the same magnitude as the advective timescale of the Weddell Gyre ($\tau_A = \frac{L}{U}$). The flow in the Weddell Gyre is of the order of 5×10^{-2}m s^{-1} (Klatt et al., 2005), and the typical length scale of the Weddell Gyre is 10^6m. This results in an advective time scale of 230 days. The relaxation timescale was tuned around this value, which resulted in a value of 200 days.

3.2 Model behaviour

Both model set ups show three general yearly cycles: it is stable for the entire year, it overturns once a year, or it overturns twice a year. The typical yearly cycles are shown in Fig. 4 where every letter stands for a regime change. The cycle starts at A, and follows the alphabetical order.

In the stable cycle we see that the model cycles between the regimes 2 and 4. At 'A' the regime transits from regime 2 to 4 because freezing temperature is reached. An increase in salinity is observed due to brine rejection. The salinity decreases when the sea ice starts to melt. At 'B' the model transits back to regime 2, because all the sea ice has melted. Due to the influence of the ocean atmospheric heat flux the temperature first rises. When the ocean atmospheric heat flux switches sign, the model cools down, until freezing temperature is reached again at 'A'.

If the model overturns once, the model overturns in regime 3. At 'A' the model transits from regime 2 to 4, and sea ice starts to grow. After a period of sea ice growth, and

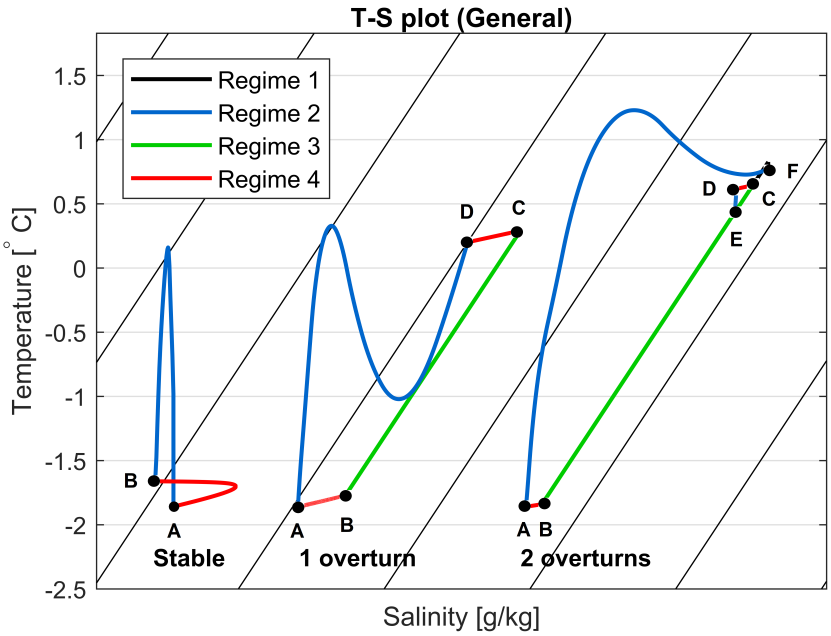

Fig. 4: The model has three general cycles: a stable cycle (left), 1 overturn (middle), and 2 overturns each year (right). The different regimes are displayed in black (1), blue (2), green (3), and red (4). The letters (A-F) represent regime changes. The cycle starts at A, and follows the alphabetical order. The black contour lines represent density, which increases from left to right. At freezing temperature ($T = -1.73°C$), ice grows and brine is rejected (A). In the stable cycle the ice eventually melts and regime 2 is entered (B). The other two cycles overturn in regime 3 (B to C), and transit immediately back to regime 4 (C). The ice melts and regime 2 is entered (D). In the cycle with two overturns, the model overturns again, but now in regime 1 (E), after which the model transits back to regime 2 (F). The model cools down until freezing temperature is reached and the cycle is repeated (A).

subsequent brine rejection in regime 4, density increases enough to cause instability at node 'B'. At 'B' the model transits from regime 4 to 3 and overturns. The mixing of the two layers causes an increase in temperature and salinity, because the warm and salty subsurface layer is more dominant due to its larger size. At 'C' stabilisation of the water column leads to a transition back to regime 4. The sea ice is quickly melted away and regime 2 is entered at 'D'. The transition 'B-C-D' happens almost instantaneously. At node 'D' a polynya has formed. The ocean atmospheric heat flux is still negative (causing cooling), but no sea ice is present. After 'D' the model cools down in the remaining part of the winter, warms again in the summer, and eventually cools down again until freezing temperature is reached at 'A'. This cycle is also shown in Martinson et al. (1981).

For the yearly cycle with two overturns, all four regimes are entered. Until node 'D' the behaviour is comparable with the cycle with only one overturn. Compared to the yearly cycle with only one overturn, less sea ice is formed. When regime 2 is entered at D, again

a polynya has formed and the surface layer starts to cool down. Due to this cooling, the density of the surface layer increases. This causes static instability of the water column leading to an overturn at node 'E'. Regime 1 is entered. In regime 1 the temperature and salinity remain relatively constant because the surface forcing becomes relatively smaller due to the increased depth of the surface layer (160m to 2000m). At 'F' the water column has stabilised again due to a decreasing density, and regime 2 is entered. After a warming period, the model cools down to freezing temperature at 'A', and the cycle is repeated.

3.3 Martinson set up

Using the 'Martinson' set up an attempt was made to reproduce the results of Martinson et al. (1981). Using the same model and parameter values, the produced results were different from the results in Martinson et al. (1981). To reproduce the results described in Martinson et al. (1981) we use a different numerical scheme in our version of the Martinson model. However, using the original numerical scheme, the original results of Martinson et al. (1981) were not reproduced. There were some problems with the documentation of the parameter values. It is for instance not clear how the heat fluxes were interpolated in the model, and no numerical parameters (the time step) were given. Therefore it was decided to use different forcing and parameter values as presented in the previous section. The general model behaviour (Fig. 4) is comparable to the results of Martinson et al. (1981). Therefore this model set up can still be used to look into the irregularity of the polynya and the importance of surface forcing. Tests with the models showed two stable solutions of the model: the model does not overturn at all (represented by case REF.1), or the model overturns twice each year (represented by case REF.2).

Cases REF.1 (Fig. 5) and REF.2 (Fig. 6) have been run for 100 years. The last 25 years are displayed, so no spin-up effects are present. Fig. 5 displays te results for REF.1. The density of both layers (Fig. 5a), the ice thickness (Fig. 5a), and a T-S plot (Fig. 5c) are shown. No overturning occurs in the entire simulation, and after the adjustment to the initial conditions (approximately 2 years for T_1 and δ and 10 years for S_1) a repeating yearly cycle is reached. This is clearly seen in the T-S plot (Fig. 5c), where the colours represent time. Only the last year is seen in the plot, since the previous years follow the same yearly cycle. The model cycles between stable regimes 2 and 4, as comparable to the stable cycle of Fig. 4. No polynyas are formed in this case.

In REF.2 (Fig. 6) the exchange coefficient K_S is increased to 2×10^{-6} ms^{-1} to initiate overturning of the model. Again the model reaches an repeating yearly cycle. However, in this case the yearly cycles are not exactly the same, which can be seen in the T-S plot (Fig. 6c). During regime 3, the last year (yellow) does not completely overlap previous

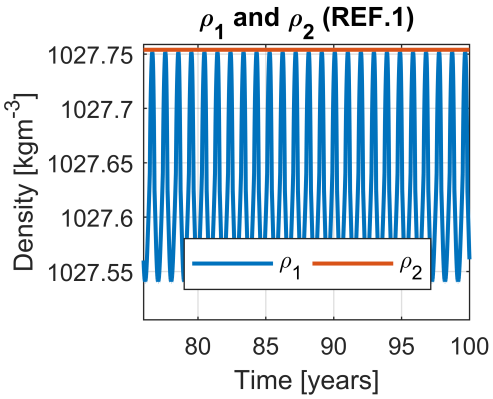

(a) Density of both layers for case REF.1.

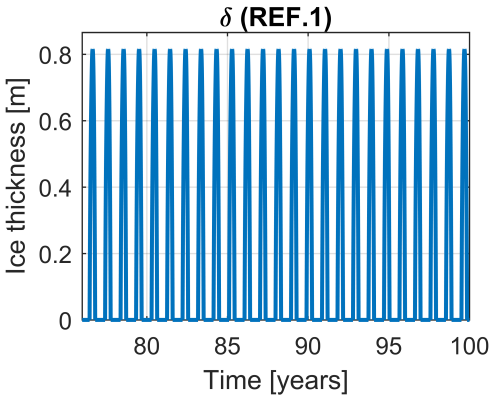

(b) Sea ice thickness for case REF.1.

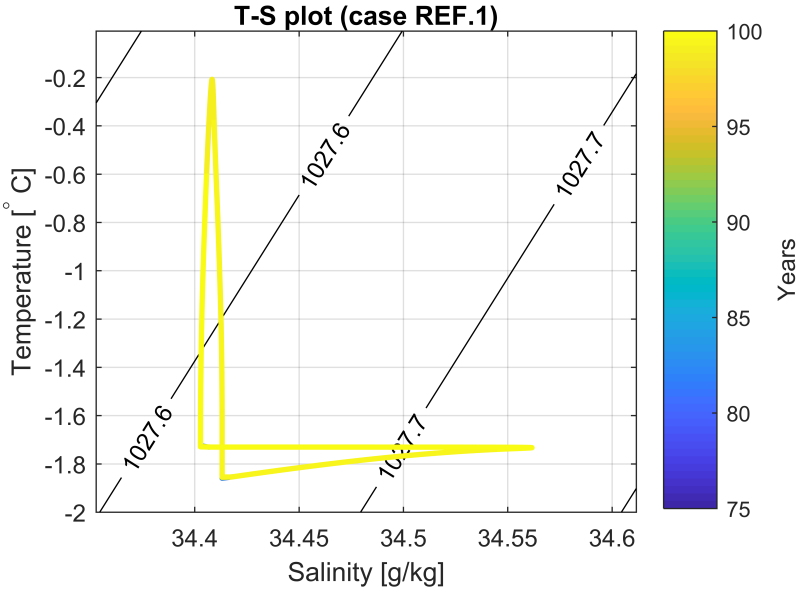

(c) T_1-S_1 plot for case REF.1.

Fig. 5: Years 76-100 for case REF.1 (Martinson set up with $K_S = 1.375 \times 10^{-6}$ ms^{-1}). (a) Density of the surface (blue) and subsurface (red) layer. (b) Sea ice thickness. (c) T-S plot of the temperature and salinity of the surface layer. Colouring of the lines represents time, ranging from year 76 (blue) to year 100 (yellow). Only the last year is visible, because previous years have the same yearly cycle. The black contour lines represent the density in kg m^{-3}.

years (visible by a small blue line to the right of the yellow line). This effect is also seen in the slowly decreasing (over time) sea ice thickness maximums (Fig. 6b). The model cycles through all four regimes. Each year the model overturns twice as seen in the yearly cycle with two overturns in Fig. 4.

These results show that this model set up is unable to switch between the non-convective and convective regime and back again. The model has two stable solutions: either it does not overturn, or it overturns twice each year. This shows that to be able to simulate periodic polynya events, more physical processes need to be included. In climate models

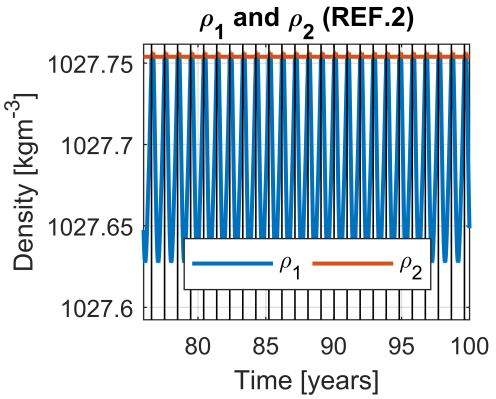

(a) Density of both layers for case REF.2.

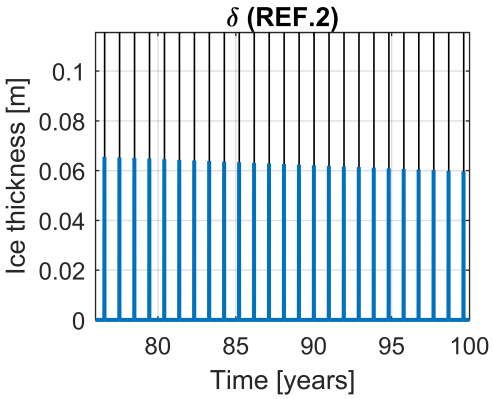

(b) Sea ice thickness for case REF.2.

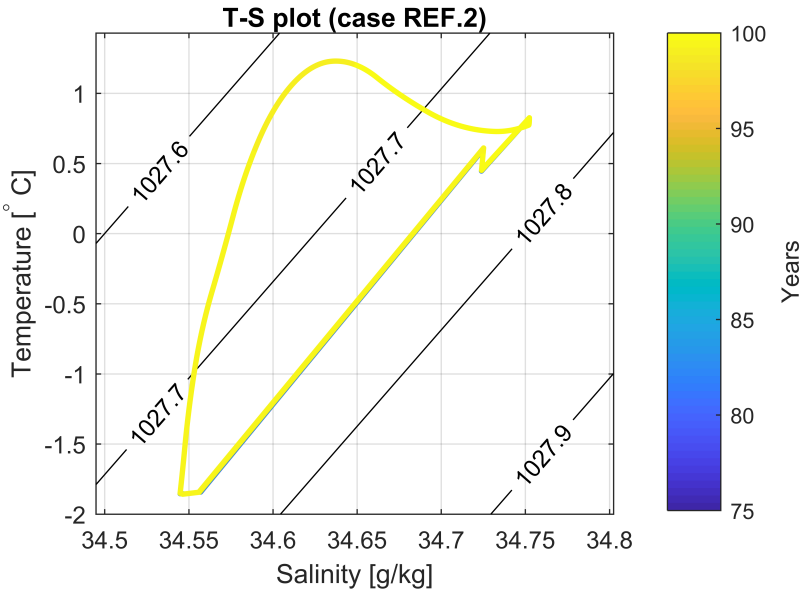

(c) T_1-S_1 plot for case REF.2.

Fig. 6: Years 76-100 for case REF.2 (Martinson set up with $K_S = 2 \times 10^{-6}$ ms^{-1}). (a) Density of the surface (blue) and subsurface (red) layer. Black lines represent overturning. (b) Sea ice thickness. Black lines represent overturning. (c) T-S plot of the temperature and salinity of the surface layer. Colouring of the lines represents time, ranging from year 76 (blue) to year 100 (yellow). Only the last year is visible, because previous years have the same yearly cycle. The black contour lines represent the density in kg m^{-3}.

heat accumulation is shown to be important for inducing overturning , and heat depletion for stabilising the water column. These processes are not present in this model set up.

3.4 Extended model

With the inclusion of periodic subsurface forcing, these additional physical processes are introduced. With this model set up, an attempt is made to reproduce the general features of van Westen and Dijkstra (2019) using a simple model. By comparing the general behaviour

of the polynya events in both models, the performance of the model can be evaluated. In van Westen and Dijkstra (2019) periodic polynya events are seen, with a periodicity of 25 years. Each 25 year period has approximately 20 non-polynya years, and 5 polynya years. The polynyas occur approximately 6 years after the subsurface heat and salt accumulation has reached its maximum. Fig. 7 displays a T-S plot of the cycle as seen in CESM. Monthly values are used, so some details are missing. The plot is based on averaged values of the surface layer (0-160m) in the polynya region (2°E - 11°E $\times$ 63.5° - 66.5°). Clear regime changes (from ice free to ice covered and back) as seen in Fig. 4 are averaged out in the CESM results, but the general feature of salinity increase during a cooling period is seen, as well as little salinity change in the warming period. Overturning in Fig. 7 is seen in the yellow lines, as a strong increase in salinity and temperature along a straight line. This is also seen in the general model behaviour (Fig. 4). Overturning in Fig. 7 do not follow the isopycnals due to the inclusion of more processes, such as diapycnal mixing, in CESM, and because only monthly values are used. A drift in the characteristics can been seen as a response to the periodic subsurface heat and salt accumulation. Both the salinity and temperature start to decrease after year 210, until year 221 when they both start to increase again until in year 231 when deep convection starts, and a polynya is formed.

The results of cases SSB, SST, and SSS are displayed in Fig. 8, 9, and 10. All cases have been run for 100 years, from which the last 25 years are shown, so no spin-up effects are presents. For each case the density of both layers, the sea ice thickness and a T-S plot of the surface layer are given.

In case SSB (Fig. 8) both subsurface fluxes are used. The effects of the background subsurface temperature and salinity on the density almost compensate each other. There is a small subsurface density maximum in the middle of a 25 year cycle (red line Fig. 8a). Periodic polynya events are simulated, however, the asymmetry in the behaviour is 7 non-polynya years against 18 polynya years. These polynyas are clearly visible by reduced sea ice thickness, but also reduced length of sea ice cover (Fig. 8b). The timing of the first polynya is approximately 4 years after the subsurface heat and salt accumulation maximum. The model shows all general yearly cycles (Fig. 8c) from Fig. 4. However, the yearly cycles do not overlap as was the case in REF.1 and REF.2. This is due to the effect of the periodic subsurface forcing on the surface layer. The same drift as in CESM (Fig. 7) is seen.

In case SST (Fig. 9) only a subsurface heat flux is used. Halfway the cycle (in Fig. 9 at 87.5 years) the density of the subsurface layer is lowest (red line Fig. 9a). The dominant period in the run is 25 years. There is no asymmetry, the time spent in the polynya period is equal to the time spent in the non-polynya period. The polynyas are visible by reduced sea ice thickness, but also reduced length of sea ice cover (Fig. 9b). The timing of first

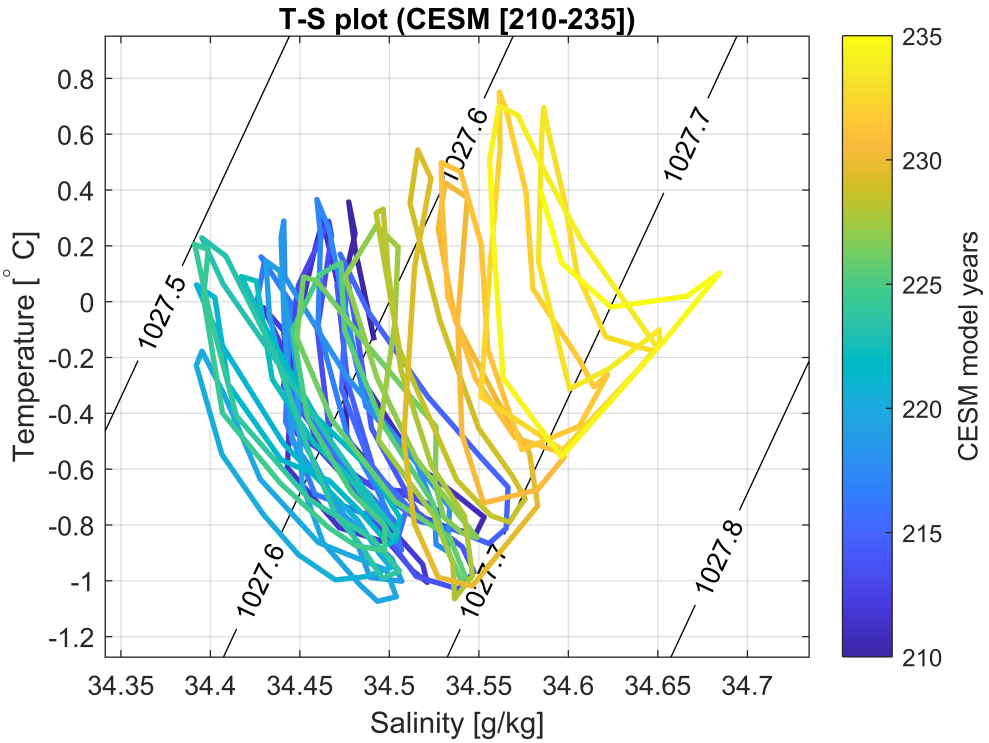

Fig. 7: T-S plot of CESM model years 210-235 from the simulation used by van Westen and Dijkstra (2019). The model is based on monthly values of the temperature and salinity averaged over the surface layer (0-160m) in the polynya region (2°E - 11°E $\times$ 63.5° - 66.5°) determined in van Westen and Dijkstra (2019). The colour coding represents time (year 210 is blue, year 235 is yellow). The polynya period captured in this plot is between years 231 and 235. The black contour lines represent density in kg m^{-3}, using a simple linear equation of state (Equation 5).

polynya is approximately 3 years before the subsurface heat accumulation maximum. This timing is before the subsurface maximum due to the effect of the subsurface forcing on the subsurface density. The subsurface forcing decreases the density, whereas in SSB the density is slightly increased. The same general yearly cycles are seen as in SSB (Fig. 9c). Again, the same drift as in CESM (Fig. 7) is seen.

In case SSS (Fig. 10) only a salt subsurface flux is used. Halfway the cycle (in Fig. 10 at 87.5 years) the density of the subsurface layer is largest (red line Fig. 10a). The same dominant period is observed. Polynyas are visible in the sea ice thickness. Not only the sea ice thickness is reduced, also the duration of ice cover has decreased (Fig. 10b). The asymmetry is 11 years in the non-polynya regime to 14 years in the polynya regime. The first overturn occurs 8 years after the maximum in the subsurface salt accumulation. The same general yearly cycles are seen as in SSB (Fig. 10c). Again, the same drift as in CESM (Fig. 7) is seen.

The general behaviour of all cases compare to the CESM simulation of van Westen and Dijkstra (2019). The dominant period in all cases is the same as in their results and

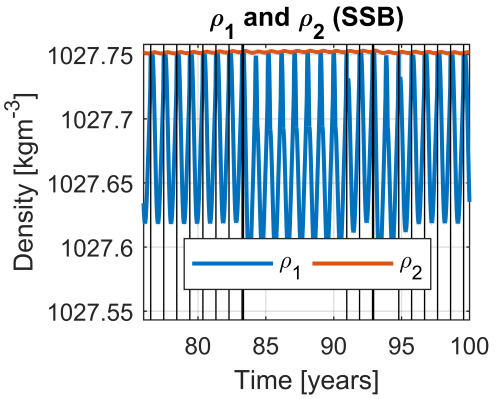

(a) Density of both layers for case SSB.

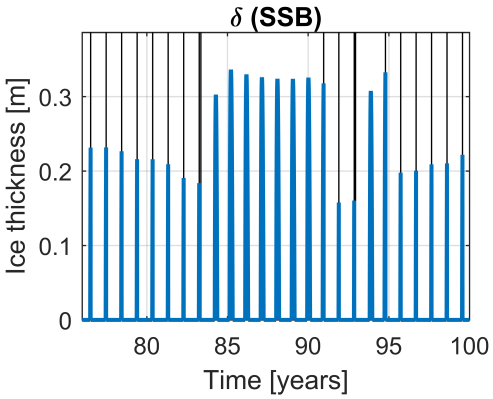

(b) Sea ice thickness for case SSB.

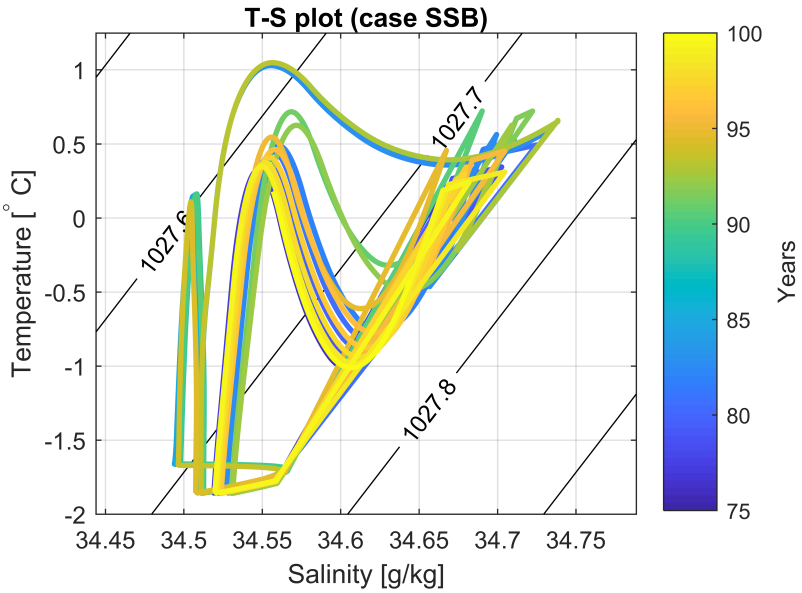

(c) T_1-S_1 plot for case SSB.

Fig. 8: Years 76-100 for case SSB ('Extended' model set up with both subsurface fluxes). (a) Density of the surface (blue) and subsurface (red) layer. Black lines represent overturning. (b) Sea ice thickness. Black lines represent overturning. (c) T-S plot of the temperature and salinity of the surface layer. Colouring of the lines represents time, ranging from year 76 (blue) to year 100 (yellow). The black contour lines represent the density in kg m^{-3}.

follows the subsurface forcing, but all cases show a different asymmetry and timing of the beginning of a polynya period. For the timing of the first polynya in a cycle, SST differs most, and SSB and SSS are 2 years off. All cases have the three general yearly cycles as presented in Fig. 4. Looking at the model results of van Westen and Dijkstra (2019), and observations (Fahrbach et al., 2011), case SSB is most complete due to the presence of both heat and salt accumulation in the subsurface layer.

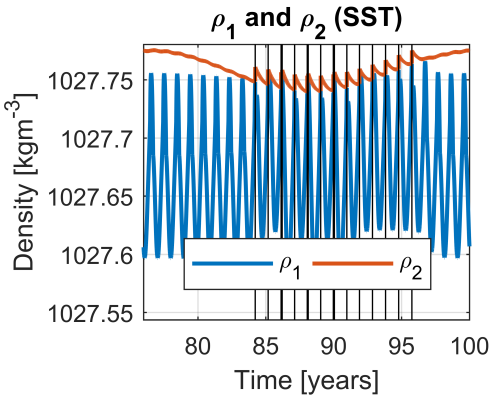

(a) Density of both layers for case SST.

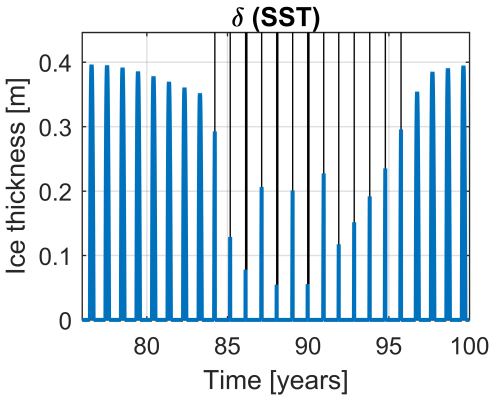

(b) Sea ice thickness for case SST.

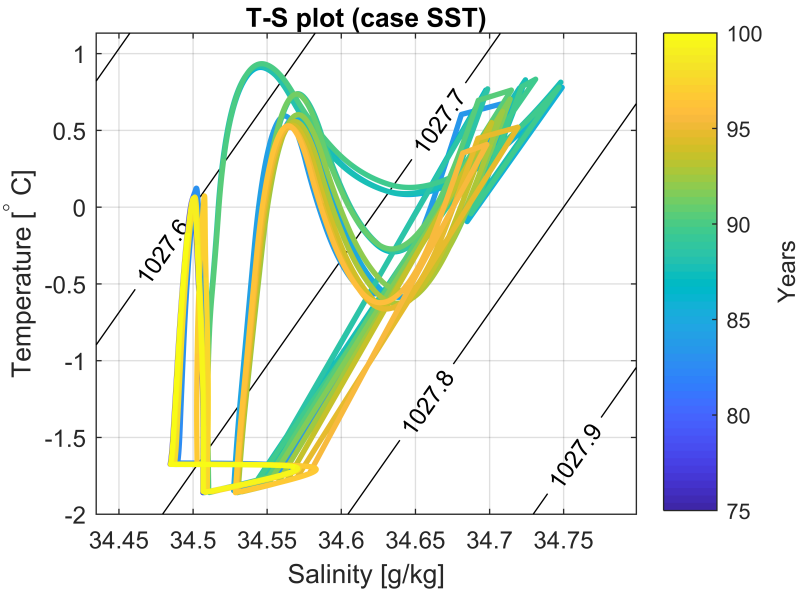

(c) T_1-S_1 plot for case SST.

Fig. 9: Years 76-100 for case SST ('Extended' model set up with only a subsurface heat flux). (a) Density of the surface (blue) and subsurface (red) layer. Black lines represent overturning. (b) Sea ice thickness. Black lines represent overturning. (c) T-S plot of the temperature and salinity of the surface layer. Colouring of the lines represents time, ranging from year 76 (blue) to year 100 (yellow). The black contour lines represent the density in kg m^{-3}.

3.5 Addition of noise

In the previous two sections we have seen that only for the subsurface model set up periodic polynya events are simulated. The period has the same size as the period of the subsurface forcing. In this section we will test whether this period is still dominant under the influence of noise. Therefore white noise is added to the freshwater flux. This has been done for case SSB, and also for case REF.1, to see whether noise can force the model in different polynya regimes. The freshwater flux has been determined from the CESM simulation of van Westen and Dijkstra (2019). From this same dataset the signal to noise ratio ($SNR = \frac{\mu^2}{\sigma^2} = 4.07$)

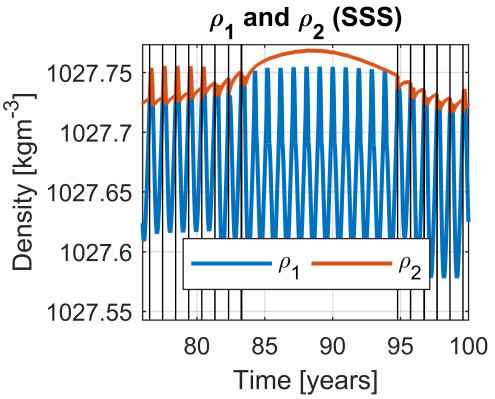

(a) Density of both layers for case SSS

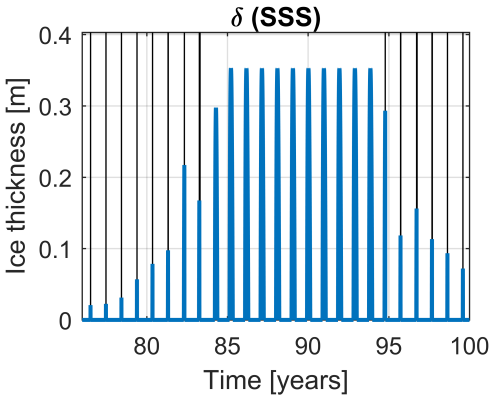

(b) Sea ice thickness for case SSS

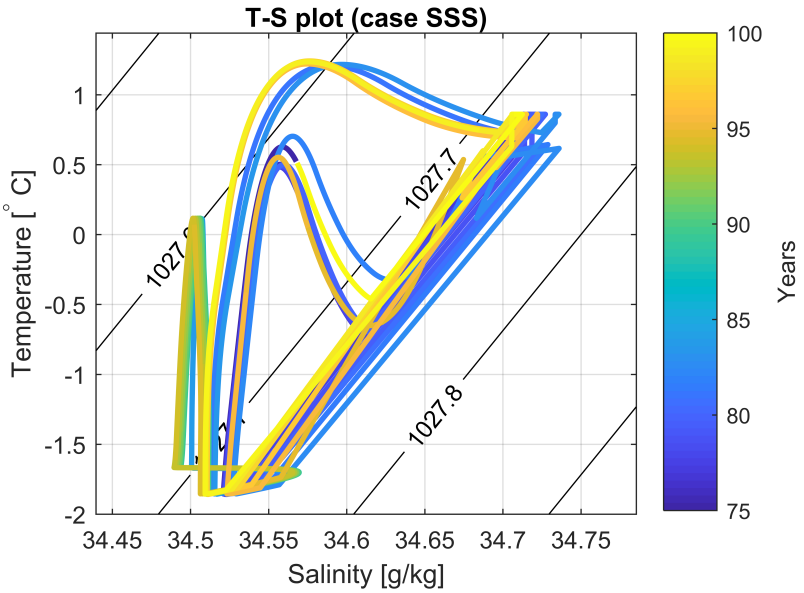

(c) T_1-S_1 plot for case SSS.

Fig. 10: Years 76-100 for case SSS ('Extended' model set up with only a subsurface salt flux). (a) Density of the surface (blue) and subsurface (red) layer. Black lines represent overturning. (b) Sea ice thickness. Black lines represent overturning. (c) T-S plot of the temperature and salinity of the surface layer. Colouring of the lines represents time, ranging from year 76 (blue) to year 100 (yellow). The black contour lines represent the density in kg m^{-3}.

was determined. Using this signal to noise ratio, a white noise signal was determined and added to the freshwater flux (F). For both cases 100 year runs were performed, from which the first 25 years were removed to remove spin up effects. Both cases have 100 ensemble members, which is thought to be enough to do a robust analysis.

Fig. 11 displays the spectral analysis on the variables T_1 (Fig. 11a), S_1 (Fig. 11b), and δ (Fig. 11c) for case SSB. In the figure the 10$^{\text{th}}$ and 90$^{\text{th}}$ percentile are plotted, as well as the mean of all runs, the median, and a randomly chosen run. For all variables we see a dominant period of 25 years, the same period as the subsurface forcing. This period

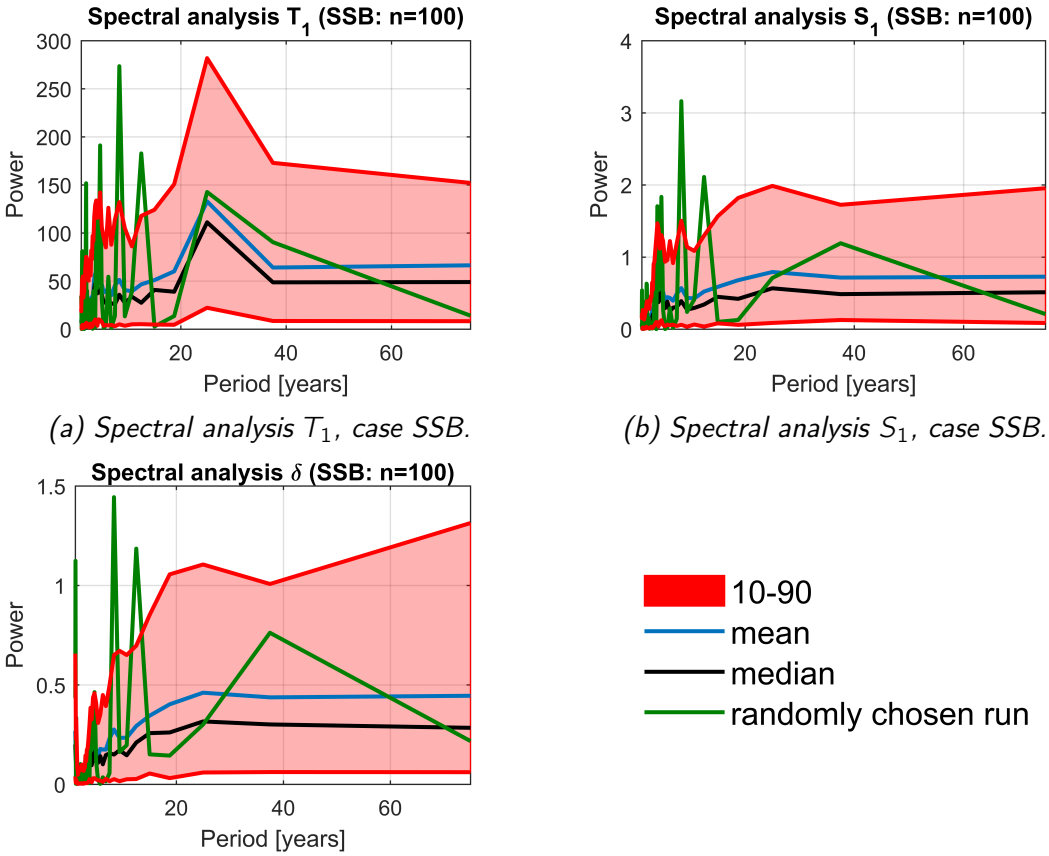

(a) Spectral analysis T_1, case SSB.

(b) Spectral analysis S_1, case SSB.

(c) Spectral analysis δ, case SSB.

Fig. 11: Spectral analysis for variables T_1 (a), S_1 (b), and δ (c) for case SSB ('Extended' model set up with both subsurface fluxes). The analysis is based on 100 ensemble members. Each ensemble member contains the last 75 years of a 100 year run to remove spin up effects. The red band represents the ensemble members between the 10^{th} and 90^{th} percentile. Also the mean (blue), median (black) and a randomly chosen run (green) are displayed.

is most dominant for the surface layer temperature. For the longer periods, the integrated effect of the white noise (red noise processes) becomes visible. This figure shows that the dominant period of 25 years is still visible with the inclusion of noise.

In Fig. 12 the spectral analysis of T_1 (Fig. 12a), S_1 (Fig. 12b), and δ (Fig. 12c) are plotted, but now for case REF.1. No clear dominant period is found. Analysis of the different runs shows that with this signal to noise ratio, the model cannot be forced from a polynya regime to a non-polynya regime. The noise only affects the timing of the first overturn. With a smaller SNR (0.1), the same applies: the model can still not be forced from a polynya regime to a non-polynya regime.

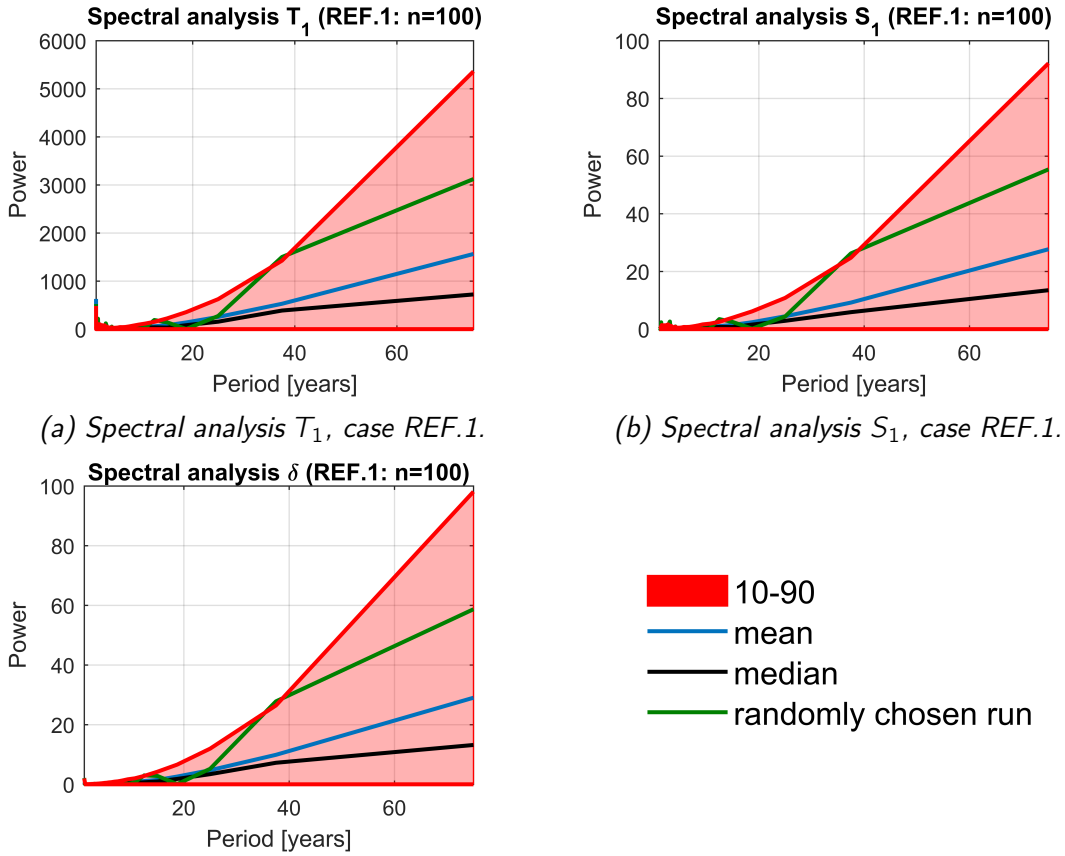

(a) Spectral analysis T_1, case REF.1.

(b) Spectral analysis S_1, case REF.1.

(c) Spectral analysis δ, case REF.1.

Fig. 12: Spectral analysis for variables T_1 (a), S_1 (b), and δ (c) for case REF.1 ('Martinson' set up with $K_S = 1.375 \times 10^{-6}\text{ms}^{-1}$). The analysis is based on 100 ensemble members. Each ensemble member contains the last 75 years of a 100 year run to remove spin up effects. The red band represents the ensemble members between the 10^{th} and 90^{th} percentile. Also the mean (blue), median (black) and a randomly chosen run (green) are displayed.

4 Summary and discussion

In this paper a new convective model, based on the model by Martinson et al. (1981), has been used to look into the Weddell Polynya. The Martinson et al. (1981) model was revisited to look into the contrast between the conclusions of Martinson et al. (1981) and van Westen and Dijkstra (2019). This research shows that the original model is not suitable to simulate multiple polynya events, which shows that some physical processes are missing in the model. The inclusion of subsurface forcing, as suggested in van Westen and Dijkstra (2019), made it possible to simulate periodic polynya events. The same period was still seen with the addition of white noise to the freshwater flux. Addition of noise to the original Martinson model did not result in multiple polynya events.

Firstly, an attempt was made to reproduce the results of Martinson et al. (1981) and to verify their conclusions. Their results were not reproduced. The general behaviour of the

model was the same, however certain details differed. The timing of the first overturn was for example earlier with respect to the results in Martinson et al. (1981). The differences can be explained by missing information in the parameter documentation. It is for instance not clear how the monthly heat fluxes are interpolated in the model. Different interpolation techniques have been used, but still, the timing of the first overturn differed with respect to Martinson et al. (1981). Another missing parameter is the used time step. Accurate time steps have been used, but still differences were found. Therefore it is also possible some parameter values were documented incorrectly. Even though the exact results were not reproduced, the general behaviour was the same. Therefore the model was still used, however a different forcing, and different parameter values were used. This set up (cases REF.1 and REF.2) was used to look at the three main conclusions of Martinson et al. (1981). The extended model set up (cases SSB, SST and SSS) was used to look at the conclusions of van Westen and Dijkstra (2019).

The first conclusion in Martinson et al. (1981) was that the deep convection is caused by brine rejection in a preconditioned surface layer. The results show that deep convection mostly starts after a short period of sea ice growth and subsequent brine rejection. Brine rejection causes a rapid increase of density in the surface layer. The results clearly show that this eventually triggers the deep convection. However, brine rejection alone cannot explain multiple polynya events (e.g. the 1970s and 2017 events), and therefore the processes controlling the preconditioning are important. However, Martinson et al. (1981) did not address the preconditioning of the surface layer. In van Westen and Dijkstra (2019) a process responsible for preconditioning of the ocean is suggested, but this is a process for the subsurface layer, and not the surface layer. van Westen and Dijkstra (2019) suggest that deep convection is caused by instabilities in the subsurface layer due to the accumulation of heat. In the extended model the polynya events are governed by the subsurface forcing. The subsurface forcing preconditions both the subsurface as the subsurface layer, after which a density increase in the surface layer due to brine rejection triggers the deep convection. The conclusion of van Westen and Dijkstra (2019) that the subsurface heat flux is more dominant than the subsurface salt flux has not been confirmed, since all extended model cases (SSB, SST, and SSS) show comparable behaviour. However, looking at the model, the subsurface heat flux has the most impact on the results. The subsurface heat flux influences every quanity (some indirectly) in the model. The subsurface salt flux only affects the density and salinity of both layers, and therefore has a much smaller influence on the results.

The second conclusion of Martinson et al. (1981) was that the WP is an irregular event. Based on our tests with the same model, we have shown that the original model is incapable

to simulate multiple events. The model has two stable solutions, it either does not overturn (case REF.1), or it does overturn each year (case REF.2). In Martinson et al. (1981) it was also shown that when the cycle becomes stable, it will remain stable, either in regimes 2 and 4, or in regimes 1 and 2. The stable solution in regime 2 and 4 can be explained by the preconditioning in the model. Preconditioning of the ocean is important. Case REF.1 probably uses a set up where the preconditioning in the ocean is insufficient to cause deep convection. The stable solution in regimes 1 and 2 can be explained by the lack of heat and salt depletion. The temperature and salinity of the subsurface layer are constant. In climate models deep convection causes the subsurface layer reservoirs to deplete, which eventually leads to stabilisation of the water column. This physical process is missing in this model set up, and therefore the model is not able to return to the non-polynya regime. However, in Martinson et al. (1981) it was possible to simulate polynyas followed by a stable, non-overturning regime. The model overturns in the first years, after which a stable, non-polynya cycle is simulated. These overturns in the first years are due to the initial conditions. When the model is adjusted to the forcing, the stable state is achieved. Our results thus correspond well to the model analysis in Martinson et al. (1981). Because the model becomes stable after a few years, irregularity cannot be assessed, since only one event can be simulated. van Westen and Dijkstra (2019) concluded that the WP is a regular, periodic event, with a dominant period of 25 years. This dominant period is related to periodic subsurface heat and salt flux related to the SOM mechanism. In our extended model periodic subsurface forcing is used. The results show periodic polynya events with the same dominant period as seen in van Westen and Dijkstra (2019). It can be concluded that periodic subsurface forcing in the extended model results in periodic polynya events with the same dominant period. This agrees with the conclusion of van Westen and Dijkstra (2019).

The final conclusion of Martinson et al. (1981) is that the polynya occurs in the Maud Rise region due to a preconditioning. This preconditioning is responsible for a decreased pycnocline depth of 150 to 250m, the depth at which the water column is most susceptible to overturning. In this study a value of 160m was used, which is inside the range of Martinson et al. (1981). However, the extended model is more sensitive than this range, which is probably due to introducing density anomalies in the subsurface layer. This makes the entire system more sensitive to density changes.

The extended model was able to capture the general features as seen in van Westen and Dijkstra (2019). However, the model is still too simplistic to accurately reproduce all features in the CESM simulation. The asymmetry in the non-polynya regime versus the polynya regime was poorly resolved. This is probably due to the difference in how

overturning is resolved. In this model the layers are either in stable stratification with a constant layer depth, or they are completely mixed. In van Westen and Dijkstra (2019) a KPP boundary mixed layer scheme is used. Resolving the growth of the mixed layer more accurately would improve the model, and possibly lead to a better representation of the asymmetry between the two regimes. Due to this instant mixing, both temperature and salinity in the surface layer increase instantly. This results in large differences after overturning with respect to the CESM simulation. Other important differences between the two models are the representation of the atmospheric and dynamical processes. In our model these processes are either prescribed (e.g. freshwater input), parameterised (e.g. upwelling) or absent (e.g. the wind field). However, even though the model is simplistic, important features were simulated. Seasonality in the yearly cycle is observed, as well as the effects of sea ice growth and melt. Periodic polynya events were simulated with the same period as the subsurface forcing. And lastly, the influence of the subsurface forcing on the surface layer, was also observed. This shows that even though not all physical processes are present in the model, the most important processes are either present or captured by good parameterisations.

Our extended model is forced by periodic subsurface fluxes related to the SOM, an intrinsic dynamical ocean mode in the Southern Ocean. This mode is mainly caused by interaction between eddies and the mean flow (Jüling et al., 2018). The SOM leads to ocean heat content anomalies in the South Atlantic ocean. These anomalies propagate with the ACC to 30°E where they enter the Weddell Gyre as WDW. Propagating along the ambient current, the anomalies eventually reach the Maud Rise region. Positive heat content anomalies lead to heat accumulation in the subsurface layer. This heat accumulation can induce deep convection, releasing the subsurface heat. In van Westen and Dijkstra (2019) the period of the polynya events was related to the period of the SOM, which is 25 years. In our extended model, subsurface fluxes related to this heat accumulation were used. The used period for the fluxes equals the periodicity of the polynya events. A possible feedback of the overturning on the SOM was not assessed in this study.

The SOM explains the period in the study of van Westen and Dijkstra (2019) and in this study. However, several climate models show irregular polynya events with no clear preferred period (Martin et al., 2013; Zanowski et al., 2015; Zhang and Delworth, 2016; Reintges et al., 2017). This is explained by the resolution of the model. Low resolution models are unable to capture the eddies that are crucial for the SOM. Therefore the SOM is not resolved. Heat accumulation is still seen in these models, but this is not related to the SOM mechanism, and therefore has not the same dominant period. Another effect of a lower resolution, is a weaker stratification (Dufour et al., 2017). A weaker stratification leads to

a system which is more sensitive to density anomalies. These anomalies can originate from anomalies in for instance the freshwater input, surface heat fluxes and subsurface fluxes. Density anomalies can induce deep convection. Without a dominant periodic forcing, in a more sensitive system, the period of deep convection becomes more irregular, which is seen in low resolution models.

In this study we looked at the importance of the surface forcing relative to the subsurface forcing. Several authors point to surface processes as the cause of deep convection in a preconditioned ocean (e.g. Martinson et al., 1981; Gordon et al., 2007). More recent studies also looked into these surface processes such as a strong cyclone (Francis et al., 2019), and advection of warm-moist air in combination with increased upwelling due to a favourable wind stress curl (Jena et al., 2019). However, studies using climate models show the importance of heat accumulation in the subsurface layer (e.g Martin et al., 2013; Latif et al., 2017; Reintges et al., 2017). This study, in combination with the study of van Westen and Dijkstra (2019), shows that subsurface accumulation of heat is one of the main drivers of the WP. Brine rejection is an important process to cause density anomalies in the surface layer. However, this is not the most dominant process, since it cannot explain the periodic return of the polynya in our model and in observations. Other surface processes, such as strong cyclones (Francis et al., 2019), eddy shedding at Maud Rise (Holland, 2001), and Taylor cap dynamics (Kurtakoti et al., 2018) are not unimportant. These effects in the Maud Rise region can be important for the duration, exact location, and size of the polynya. However, we suggest that subsurface processes are most dominant and govern the initial formation and periodicity of the Weddell Polynya.

References

Alverson, K., Owens, W.B., 1996. Topographic Preconditioning of Open-Ocean Deep Convection. J. Phys. Oceanogr. 26, 2196–2213. doi:10.1175/1520-0485(1996)026<2196:TPOOOD>2.0.CO;2.

Carsey, F.D., 1980. Microwave Observations of the Weddell Polynya. Mon. Weather Rev. 108, 2032–2044. doi:10.1175/1520-0493(1980)108<2032:MOOTWP>2.0.CO;2.

Cheon, W.G., Gordon, A.L., 2019. Open-ocean polynyas and deep convection in the Southern Ocean. Sci. Rep.-UK 9. doi:10.1038/s41598-019-43466-2.

Dufour, C.O., Morrison, A.K., Griffies, S.M., Frenger, I., Zanowski, H., and co-authors, 2017. Preconditioning of the Weddell Sea polynya by the ocean mesoscale and dense water overflows. J. Climate 30, 7719–7737. doi:10.1175/JCLI-D-16-0586.1.

Fahrbach, E., Hoppema, M., Rohardt, G., Boebel, O., Klatt, O., and co-authors, 2011. Warming of deep and abyssal water masses along the Greenwich meridian on decadal time scales: The Weddell gyre as a heat buffer. Deep-Sea Res. Pt. II 58, 2509–2523. doi:10.1016/j.dsr2.2011.06.007.

Francis, D., Eayrs, C., Cuesta, J., Holland, D., 2019. Polar cyclones at the origin of the reoccurrence of the Maud Rise Polynya in austral winter 2017. Journal of Geophysical Research: Atmospheres 0. doi:10.1029/2019JD030618.

Gordon, A.L., Viscbeck, M., Comiso, J.C., 2007. A Possible Link between the Weddell Polynya and the Southern Annular Mode. J. Climate 20, 2258–2571. doi:10.1175/JCLI4046.1.

Holland, D.M., 2001. Explaining the Weddell Polynya - a Large Ocean Eddy Shed at Maud Rise. Science 292, 1697–1700. doi:10.1126/science.1059322.

Jena, B., Ravichandran, M., Turner, J., 2019. Recent Reoccurrence of Large Open-Ocean Polynya on the Maud Rise Seamount. Geophysical Research Letters 46, 4320–4329. doi:10.1029/2018GL081482.

Jüling, A., Viebahn, J.P., Drijfhout, S.S., Dijkstra, H.A., 2018. Energetics of the Southern Ocean Mode. Journal of Geophysical Research: Oceans 123, 9283–9304. doi:10.1029/2018JC014191.

Klatt, O., Fahrbach, E., Hoppema, M., Rohardt, G., 2005. The transport of the Weddell Gyre across the Prime Meridian. Deep Sea Research Part II: Topical Studies in Oceanography 52, 513–528. doi:https://doi.org/10.1016/j.dsr2.2004.12.015.

Klopfenstein, R.W., 1971. Numerical differentiation formulas for stiff systems of ordinary differential equations. RCA Rev. 32, 447–462.

Kurtakoti, P., Veneziani, M., Stössel, A., Weijer, W., 2018. Preconditioning and Formation of Maud Rise Polynyas in a High-Resolution Earth System Model. J. Climate 31, 9659–9678. doi:10.1175/JCLI-D-18-0392.1.

Latif, M., Martin, T., Reintges, A., Park, W., 2017. Southern Ocean Decadal Variability and Predictability. Curr. Clim. Change Rep. 3, 163–173. doi:10.1007/s40641-017-0068-8.

Le Bars, D., Viebahn, J.P., Dijkstra, H.A., 2016. A Southern Ocean mode of multidecadal variability. Geophys. Res. Lett. 43, 2102–2110. doi:10.1002/2016GL068177.

Lindsay, R.W., Holland, D.M., Woodgate, A., 2004. Halo of low ice concentration observed over the Maud Rise seamount. Geophys. Res. Lett. 3, 1–4. doi:10.1029/2004GL019831.

Martin, T., Park, W., Latif, M., 2013. Multi-centennial variability controlled by Southern Ocean convection in the Kiel Climate Model. Clim. Dynam. 40, 2005–2022. doi:10.1007//s00382-012-1586-7.

Martinson, D.G., Killworth, P.D., Gordon, A.L., 1981. A Convective Model for the Weddell Polynya. J. Phys. Oceanogr. 11, 466–488. doi:10.1175/1520-0485(1981)011<0466:ACMFTW>2.0.CO;2.

Parkinson, C.L., 1983. On the Development and Cause of the Weddell Polynya in a Sea Ice Simulation. J. Phys. Oceanogr. 13, 501–511. doi:10.1175/1520-0485(1983)013<0501:OTDACO>2.0.CO;2.

Reintges, A., Martin, T., Latif, M., Park, W., 2017. Physical controls of Southern Ocean deep-convection variability in CMIP5 models and the Kiel Climate Model. Geophys. Res. Lett. 44, 6951–6958. doi:10.1002/2017GL074087.

Shaw, W.J., Stanton, T.P., 2014. Dynamic and Double-Diffusive Instabilities in a Weak Pycnocline. Part I: Observations of Heat Flux and Diffusivity in the Vicinity of Maud Rise, Weddell Sea. J. Phys. Oceanogr. 44, 1973–1991. doi:10.1175/JPO-D-13-042.1.

Weijer, W., Veneziani, M., Stössel, A., Hecht, M.W., Jeffery, N., and co-authors, 2017. Local atmospheric response to an open-ocean polynya in a high-resolution climate model. Journal of Climate 30, 1629–1641. doi:10.1175/JCLI-D-16-0120.1.

van Westen, R.M., Dijkstra, H.A., 2017. Southern Ocean origin of multidecadal variability in the North Brazil Current. Geophys. Res. Lett. 44, 10541–10548. doi:10.1002/2017GL074815.

van Westen, R.M., Dijkstra, H.A., 2019. Mechanisms of Multidecadal Variability in the Southern Ocean. Submitted .

Zanowski, H., Hallberg, R., Sarmiento, J.L., 2015. Abyssal Ocean Warming and Salinification after Weddell Polynyas in the GFDL CM2G Coupled Climate Model. J. Phys. Oceanogr. 45, 2755–2772. doi:10.1175/JPO-D-15-0109.1.

Zhang, L., Delworth, T.L., 2016. Impact of the Antarctic bottom water formation on the Weddell Gyre and its northward propagation characteristics in GFDL CM2.1 model. Journal of Geophysical Research: Oceans 121, 5825–5846. doi:10.1002/2016JC011790.